POLITECNICO DI TORINO

Thesis for M.Sc. programme in Physics of Complex Systems

Active phase separation on cell membranes

Supervisor
Andrea Antonio Gamba
Carla Bosia

Candidate
Alessandra Putgioni

Anno Accademico 2023-2024

Abstract

The spatial organization of cellular membranes is crucial for intracellular trafficking processes, where membrane-bound Rab GTPases play a central role. This study explores the formation and dynamics of Rab protein domains, focusing specifically on Rab5 and Rab11, and examines their structural organization and functional roles in endosomal trafficking. Rab proteins act as molecular switches that regulate distinct stages of the endocytic pathway by recruiting various effectors, thereby orchestrating vesicle transport. Building on previous studies of Rab5/Rab7 domains, we develop a computational model to simulate the formation of Rab5/Rab11 domains. Our simulations demonstrate how, starting from a homogeneous distribution, interactions and reactions among Rab5 and Rab11 proteins lead to the emergence of distinct domains, enhancing our understanding of membrane compartmentalization in cellular trafficking. Using high-resolution imaging and advanced quantitative analyses, we characterize the clustering patterns of Rab domains and their association with specific membrane compartments. A Statistical Object Distance Analysis analysis (SODA) is used. This method allows to analyze the spatial relationships between molecular positions. We analyzed two sets of experiments on cells treated with PI3-kinase class III inhibitor Vps34-IN1 and microtubole inhibitor Nocodazole to investigate the impact of these compounds on Rab domain formation.

Contents

1 Introduction

Endocytosis is the cellular process by which cargo molecules are transported into the cell's interior within membrane-bound vesicles. All known endocytic pathways can be classified into two main types: clathrin-mediated endocytosis (CME) and clathrin-independent endocytosis.

Clathrin-mediated endocytosis involves cells that absorb molecules through the inward growth of the plasma membrane facilitated by clathrin proteins. In contrast, clathrin-independent endocytosis is regulated by different signals and factors, providing cells with a wider range of regulatory options.

Internalized cargo is directed to a common early endosome (EE, also known as the sorting endosome), a population of small vesicles and tubules, where it is sorted for onward transport to different cellular destinations. EE is mildly acidic, which facilitates the release of some ligands from their receptors. The cargo can then progress along the degradative pathway or be returned to the plasma membrane. The majority of ligands that are internalized will undergo degradation by collecting in the lumen of the EE so that they can be sorted into late endosomes and finally into lysosomes where they are degraded. Recycling back to the plasma membrane can occur directly from the EE (the fast recycling pathway) or indirectly through a distinct subpopulation of recycling endosomes (REs), the endosomal recycling compartment (ERC), in a slow recycling pathway.

The composition of the plasma membrane is controlled by the balance between endocytosis and recycling, and it is emerging that the disruption of this balance contributes to a wide range of diseases including cancer and neurodegenerative disorders. Such a dynamic system needs to be tightly regulated to ensure that the right cargo gets to the right location at the right time.

Members of the Rab family of small GTPases play an important role in the regulation of this system [12].

Rab GTPases represent the largest family of small GTPases, which function as molecular switches that alternate between two conformational states: the GTP-bound "on" form (active state) and the GDP-bound "off" form (inactive state). This state alternation is crucial for cell regulation, as active Rab GTPases interact with a variety of effectors to coordinate the direction and timing of vesicular transport and endosomal compartment organization.

Rab activation occurs through the exchange of GDP for GTP, a process catalyzed by specific guanine nucleotide exchange factors (GEFs). GEFs recognize inactive Rab proteins and promote the replacement of GDP with GTP, causing a conformational change that shifts Rab to the active state.

Once Rab has fulfilled its function, it transitions back to the GDP-bound (inactive) state through the hydrolysis of GTP to GDP, a reaction catalyzed by GTPase-activating proteins (GAPs). This cycle between active and inactive states enables Rab proteins to act as molecular "timers", providing regulated timing for vesicular trafficking and contributing to the dynamic organization of the cell membrane and intracellular transport pathways.

A number of studies have demonstrated that different Rab proteins, when localised on the same organelle, occupy distinct membrane microdomains, which are often referred to as Rab domains. [4, 15, 3, 14].

Cargo is transported through discrete and specialised domains on endosomes, each characterised by the presence of specific Rab proteins, thereby indicating a high degree of compartmentalisation within the membrane structure. The pharmacological sensitivities of these membrane domains reflect their distinct biochemical compositions and functional roles in cellular processes. A number of observations indicate that mechanisms exist for the lateral segregation of Rab GTPases into membrane domains with specialised functions.

The most plausible mechanism behind this segregation appears to involve, at least in part, the activity of effector proteins that help to maintain the distinctiveness of each Rab domain [14]. For instance, positive feedback loops involving Rab effectors containing guanine nucleotide exchange factors (GEFs) for Rab GTPases contribute to the amplification of local Rab activation and enrichment. These feedback loops ensure that specific Rab GTPases are concentrated in particular membrane microdomains, thereby enhancing their functional specificity and effectiveness.

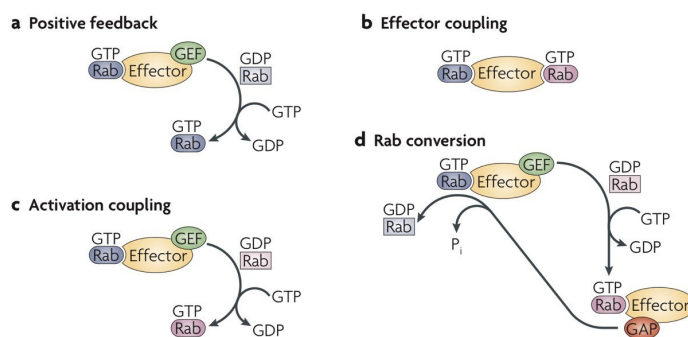Figure 1 shows some other examples of Rab dynamics.

Figure 1: Figure from [14]. Coordination of rab functions. **a)** Positive-feedback loops are created when a Rab effector complex contains GEFs, which catalyse the exchange of GDP for GTP, for the same Rab GTPase that recruits them in the first place. **b)** Rab effectors frequently contain separate binding sites for two Rab GTPases, enabling tethering between two membranes or coordination of microdomains in the same membrane. **c)** When a GEF for a second Rab is included in the effector complex of the first Rab GTPase, the second Rab will be activated through the conversion from a GDP-bound form to a GTP-bound form. **d)** The effector complex of the secondarily activated Rab GTPase might contain a GAP for the first Rab GTPase. This GAP can hydrolyse the GTP on the first Rab, thereby converting the Rab to the GDP-bound form and releasing an inorganic phosphate (Pi)

In a study [15], focused on the analysis of Rab4, Rab5 and Rab11 it was demonstrated that these domains are dynamic but do not significantly intermix over time and the overall distribution of Rab4, Rab5, and Rab11 domains on endosomes does not significantly change at different stages of recycling. With regard to Rab proteins, both early and recycling endosomes are structured into Rab4, Rab5, and Rab11 domains, only the relative amounts of these domains differ. Early endosomes situated at the cell periphery are predominantly constituted by Rab5 and Rab4 domains, with a paucity of Rab11 domains. In contrast, recycling endosomes in the pericentriolar region are predominantly composed of Rab4 and Rab11 domains. Rab5 is essential for the transport of material from the plasma membrane to early endosomes, as well as homotypic endosome fusion. It is predominantly present in globular domains, rather than in tubules or vesicles. Rab11 has been identified in the recycling endosome, the trans-Golgi network and in the specialized storage membranes of regulated secretory pathways. Rab11 was observed to be present in the pericentriolar region, as well as on small vesicular structures distributed throughout the cytoplasm.

Early endosomes are composed of globular and tubulovesicular membrane elements, which have been proposed to reflect different functional domains.

The authors traced the path of transferrin through various endosomal domains labeled with Rab4, Rab5, and Rab11, discovering that these Rab proteins occupy specific sub-regions within the endosomes. This suggests a specialized organization of endosomal membranes based on function, where Rab4, Rab5, and Rab11 respectively regulate the fast, early, and late pathways of transferrin trafficking and recycling. The analysis of these three different Rab proteins confirmed the hypothesis that the continuous membrane is organized into distinct domains. These domains can be formed by individual Rab proteins, by the overlap between two of them, or by the combination of all three. The lowest overlap was seen with Rab5 and Rab11.
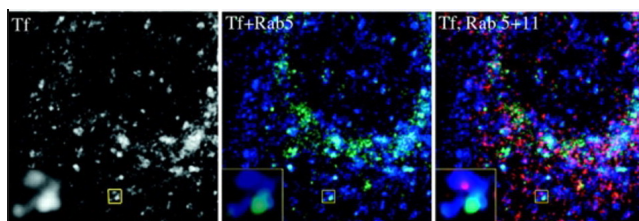

Figure 2: Figure from [15]. Confocal image of Rab5 and Rab11 labeling on transferrin-filled endosomes. A431 cells expressing CFP-Rab5 and YFP-Rab11 after internalization of Texas red transferrin for 30 min

In addition to regulating the nucleotide cycle and coordinating activity within Rab domains, GEFs, GAPs and effectors can bind to multiple Rab GTPases, thereby facilitating the progression of cargo between Rab domains along the endocytic pathways. The transportation of cargo occurs in a sequential manner along the recycling route, from the Rab5 to the Rab4 and Rab11 domains, and along the degradative route, from the Rab5 to the Rab7 domains.

In order to gain insight into the mechanisms of organelle biogenesis and the cargo transport that underpins it, it is essential to study the constitution of domains and the manner in which they interact with one another. A considerable number of cellular functions are dependent on functional modules that interact with one another via Rab GTPases.

In order to guarantee the effective coordination and regulation of these disparate functions, communication between neighbouring domains is imperative. The inter-domain communication is facilitated by the utilisation of shared effector molecules, which act as molecular bridges between adjacent Rab proteins, thereby enabling synchronised activity and maintaining the functional integrity of the endocytic network. To illustrate, a mechanism designated as Rab conversion encompasses the recruitment of a guanine nucleotide exchange factor (GEF) for a specific Rab GTPase by an upstream GTPase. The transition of early endocytic structures marked by Rab5 into later structures marked by Rab7 has been clearly demonstrated. Mathematical models indicate that Rab5 maintains its activation of Rab7 until Rab7 reaches a critical threshold, at which point it initiates the inactivation of Rab5 through a negative feedback loop. It seems probable that this loop involves the recruitment of a Rab5 GAP by Rab7, thereby creating a self-regulating system. This feedback mechanism, which has been likened to an electrical circuit breaker, ensures that Rab5 is rapidly inactivated once GTP-bound Rab7 has reached the requisite level. This allows for a swift and controlled transition between Rab5 and Rab7 activities.

Although Rab5 is indispensable for the development of early endosomes, its diminution is also crucial for the transfer of cargo to the late endocytic pathway. The endosomal system can be conceptualised as an integrated and dynamic network of Rab domains, each with a distinctive biochemical composition, engaged in dynamic interactions with one another. The data indicate that Rab domains are organised in a way that avoids overlap and allows for the maintenance of distinct functions, either through physical separation or dynamic conversion mechanisms.

In light of this mechanism, it seems feasible to propose a model of endocytic transport based on discrete yet functionally interconnected modular units or modules. Figure 3 depicts a reaction scheme proposed by [4] for the Rab5/Rab7 model. This model comprises two Rab modules, each containing regulators that control the transition of Rab GTPase between active and inactive states, as well as effectors that bind to active Rab and facilitate its involvement in specific functions, including those related to vesicular transport.

The two modules are then linked by positive and negative feedback loops based on established or proposed molecular interactions [4].
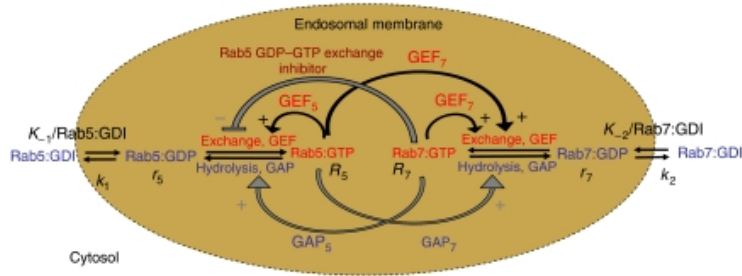
8

Figure 3: Figure from [4]. Reaction scheme of membrane recruitment and GDP/GTP cycle of two Rab GTPases, Rab5 and Rab7. The scheme shows that, during the conversion process, the two Rab GTPases, together with GEFs, GAPs and effectors, form two interconnected modules on the same endosome membrane. Initially, the endosome membrane is enriched in Rab5 and depleted of Rab7. Upon conversion, the membrane composition is reversed, that is, Rab7 prevails over Rab5. GEFs catalyse the exchange of GDP with GTP, and GAPs catalyse the hydrolysis of GTP into GDP ([17]), acting upon the respective Rab proteins (GEF5 for Rab5, GEF7 for Rab7, GAP5 for Rab5, GAP7 for Rab7). GEFs and GAPs acting on one Rab protein may also be part of effector complexes, binding the active conformation of the same or the other Rab species. Black curved arrows denote known (biochemically demonstrated) feedback mechanisms on Rab activation whereas grey arrows represent potential, but yet hypothetical, negative feedback mechanisms. The - and + signs denote a decrease or increase in the reactions.

2 Physics of cell membrane pattering

The process of symmetry breaking is a pivotal mechanism in biological systems, whereby cells can organise themselves into well-defined structures and undergo functional diversification. [9]. The Rab proteins, which switch between their active and inactive forms, and the interactions between different Rabs, thanks also to their effectors, form feedback loops that are crucial for the generation and maintenance of asymmetries.

The ordering of similar molecules by mutual affinity in spatially separated domains is driven by the interplay of attractive and repulsive interactions. The formation of these domains is contingent upon the action of electrostatic interaction exceeding the thermal agitation. The initial stage is referred to as nucleation and occurs as a result of stochastic fluctuations (homogeneous nucleation) or due to the presence of a sufficiently large nucleation centre in response to an external perturbation (heterogeneous nucleation). In the case of a limited pool of molecules, a process of coarsening occurs, whereby the larger domains grow at the expense of the smaller ones until an equilibrium situation is reached. This is due to competition between the different domains. During the process, the interface area between the two phases is reduced, resulting in the formation of spherical domains. A critical size exists below which domains are unstable and tend to disappear [5]. In biological systems, the reactions occur in an out-of-equilibrium context, which permits the existence of a diverse range of steady states.

The present work is based on a model for active phase separation on cell membranes, which has been previously used to describe chemotactic polarization [Rif. [6]].

The simplest case is that of a reaction-diffusion system comprising two types of molecules, A and B, which exhibit homotypic intermolecular affinity and are capable of mutual conversion. [13]. The process begins with a well-mixed phase, wherein islands of A and B molecules nucleate and grow in a sea of well-mixed phase.

In order for the mutual conversion to occur, the system also contains enzymes that facilitate the conversion A $\rightarrow$ B (E_B^*) and B $\rightarrow$ A (E_A^*) which bind to the molecules on the membrane.Furthermore, this enzyme is capable of shuttling between the membrane and the cytosol (E_A, E_B).

It is assumed that the rate of diffusion in the cytosol and the rate of diffusive shuttling from the cytosol to the membrane are both significantly faster than the rate of lateral diffusion for the particles on the membrane.

Only the mutual conversion is possible for A and B, they cannot begin created or destructed, so the total number of molecules is assumed to be constant It is only possible for A and B to undergo mutual conversion; neither can be created nor destroyed. Therefore, the total number of molecules is assumed to be constant (A+B = c).

The reactions present in the system (see fig. 4) can be describer as a system of differential equations using mass-action kinetic approach:

1. $\frac{\partial E_B}{\partial t} = k_B^d E_B^* - k_B^a E_B B$

2. $\frac{\partial E_A}{\partial t} = k_A^d E_A^* - k_A^a E_A A$

3. $\frac{\partial E_B^*}{\partial t} = D\Delta E_B^* - k_B^d E_B^* + k_B^a E_B B$

4. $\frac{\partial E_A^*}{\partial t} = D\Delta E_A^* - k_A^d E_A^* + k_A^a E_A A$

5. $\frac{\partial B}{\partial t} = D\Delta B + g(A, B, E_A^*, E_B^*)$

6. $\frac{\partial A}{\partial t} = D\Delta A - g(A, B, E_A^*, E_B^*)$

Where:

- $g(A, B, E_A^*, E_B^*) = k_B^c \frac{A E_B^*}{K_{m,A}+A} - k_A^c \frac{B E_A^*}{K_{m,B}+B}$ describes the enzymatic conversion of A and B.

- Δ *is the Laplace-Beltrami operator on the curved membrane surface*

- *D is the diffusivity (assumed to be equal for all the species).*

This assumption holds because when the enzymes are bound to the species diffuse at the same velocity of the molecules (while in the cytosol diffuse much faster). The enzymatic reactions are described by Michaelis-Menten equation, where we can assume K to be the same.

The conservation law allows to rewrite the system dynamics in term of a single order parameter:

$$\phi = A - B$$

Substrating eq. 5 to 6 :

$$\frac{\delta\phi}{\delta t} = D\Delta\phi - 2g(\phi) \qquad [7]$$

Since diffusion in the cytosol is much faster than diffusion on the membrane, let us consider the limit where diffusion in the cytosol is infinite, and therefore the distribution of enzymes in the cytosol can be considered as uniform. Also the process of association-dissociation of the enzymes to the membrane is fast, and in approximately stationary state. In this way we obtain:

$$E_B^* = \frac{k_B^a}{k_B^d} E_B B$$

$$E_A^* = \frac{k_A^a}{k_A^d} E_A A$$

11

Inserting these results in eq. 7 we find:

$$\frac{\delta \phi}{\delta t} = D\Delta\phi + f(\phi)$$

Where

$$f(\phi) = -(c^2 - \phi^2)[\beta h(\phi) - \alpha h(-\phi)]$$

with

$$\alpha = \frac{k_A^c k_A^a}{k_A^d} E_A, \quad \beta = \frac{k_B^c k_B^a}{k_B^d} E_B, \quad h(\phi) = \frac{1}{2K_m + c + \phi}$$
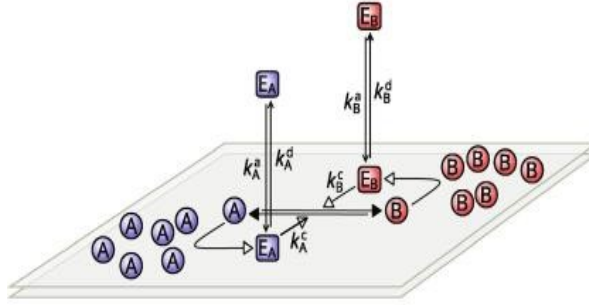

Figure 4: Figure from [5]. Abstract model for active phase separation on lipid membranes

Rab GTPases alternate between two states: an active state and an inactive state. The transition between these states is regulated by specific GAPs and GEFs, which function through feedback mechanisms. To investigate this process, it can be modeled using 1 to 6 equations. The following chapter will analyse two Rabs models: the Rab 5 model and the Rab5/Rab11 model.

3 Theoretical models of membrane patterning

3.1 A model for Rab5 activation

In light of the model delineated in the preceding chapter, it is feasible to derive a reaction-diffusion system comprising Rab proteins. The protein may exist in either an active or inactive state. The transition between the active and inactive states of the protein is contingent upon the presence of guanine nucleotide exchange factors (GEFs) and GTPases-activating proteins (GAPs).

The reactions characterising the model are principally three:

1. Dissociation

2. Association

3. Catalysis

The aforementioned general model allows for the reconstruction of the evolution of a biochemical network, provided that the input quantities are specified, the reactions involved in the process are identified, and the appropriate rates are given.

To illustrate, it is feasible to envisage the formation of $Rab5^{GTP}$ (the active form of Rab5) domains on a membrane. It has been demonstrated on numerous occasions that positive feedback enables the activation of Rab5 and the formation of domains on the membrane, beginning with a well-mixed system [1] . The membrane-bound $Rab5^{GTP}$ can act as a seed for Rab5 activation, as $Rab5^{GTP}$ bound to the correct GEF (in this case Rabex5) enables Rab5 to be activated through a catalytic reaction. This mechanism is made possible by the action of an effector called Rabptin5, which activates Rabex5. The binding of Rabaptin5 to Rab5 serves to further facilitate the activation of additional Rab5s. This is achieved by interacting with Rabex5 (the GEF of Rab5), thereby creating a positive feedback loop that amplifies the recruitment of Rab5 and Rabaptin5 to endosomal domains. It has been postulated that these GEF/effector interactions represent a general mechanism for domain formation and symmetry breaking.
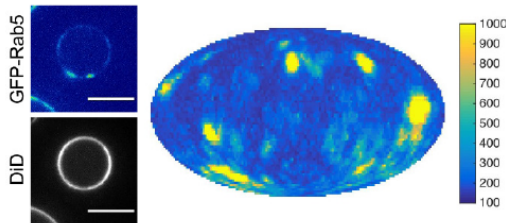

Figure 5: Reconstruction of Rab5 domains in vitro from [3].

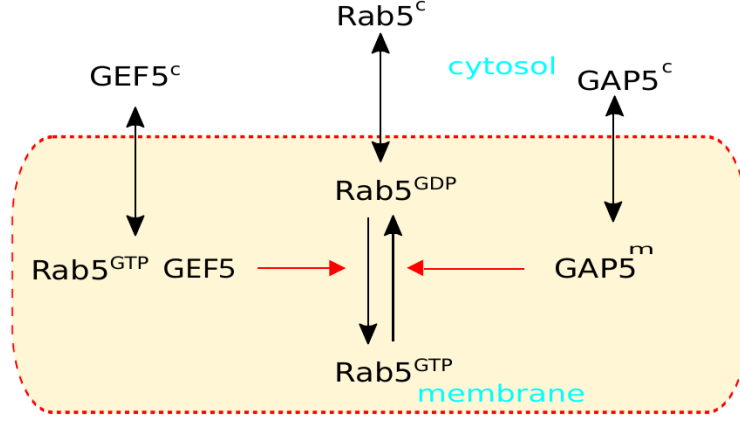The reactions characterising this model are schematised in the figure below:

Figure 6: Representation of a model with a single Rab5

This model reaction is based on the interaction of a single protein. The protein is capable of diffusing through the membrane into the cytosol, and vice versa. Additionally, GAP5 is capable of diffusing from the cytosol to the membrane, facilitated by the presence of binding sites that may potentially lead to the deactivation of Rab5a in the membrane. The reverse reaction is facilitated by the binding of Rab5a to GEF5, which results in the activation of other Rab5 molecules in a GDP-bound state.

The stochastic implementation of the reactions characterising the Rab5 model is achieved through the utilisation of a Gillespie algorithm. In this instance, the following reactions are under consideration:

$Rab5^{GTP}{:}\text{GEF5} \rightleftharpoons Rab5^{GTP}{+}\text{GEF5}$	dissociation/association	k_E^d / k_E^a
$Rab5^{GDP} \rightleftharpoons Rab5^{GDP}(\text{c}){+}\text{binding site}$	dissociation/association	$k_{b.s}^d / k_{b.s}^a$
$\text{GAP5(m)} \rightleftharpoons \text{GAP5(c)}{+}\text{b.s}$	dissociation/association	k^D
$Rab5^{GTP} \rightarrow Rab5^{GDP}$	catalysis	k_1^c, K_m
$Rab5^{GDP} \rightarrow Rab5^{GTP}$	catalysis	k_2^c, K_m

Table 1: List of reactions in the biochemical network (Rab5)

Every reaction is characterised by a diffusion rate.

In particular, for the Rab5 model the reaction rates are derived by the following work [1]. This study analyses the Rab5 activation network, describing a system consisting of the reactions listed in Table 2 and the corresponding coefficients (fig. 7).
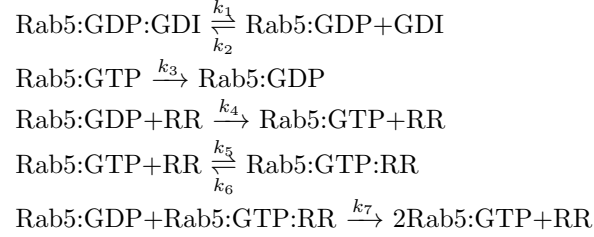
$$\text{Rab5:GDP:GDI} \overset{k_1}{\underset{k_2}{\rightleftharpoons}} \text{Rab5:GDP+GDI}$$

$$\text{Rab5:GTP} \overset{k_3}{\longrightarrow} \text{Rab5:GDP}$$

$$\text{Rab5:GDP+RR} \overset{k_4}{\longrightarrow} \text{Rab5:GTP+RR}$$

$$\text{Rab5:GTP+RR} \overset{k_5}{\underset{k_6}{\rightleftharpoons}} \text{Rab5:GTP:RR}$$

$$\text{Rab5:GDP+Rab5:GTP:RR} \overset{k_7}{\longrightarrow} 2\text{Rab5:GTP+RR}$$

Table 2: Rections described by the model of [1] (RR stands for Rabex5:Rabaptin5 complex).

Parameter	Value	Notes
k_1	$1.2 \times 10^{-1}\ s^{-1}$	Fitted parameter from estimated $K_d = k_1/k_2 = 6$ μM (20).
k_2	$2.25 \times 10^5\ M^{-1}s^{-1}$	Fitted parameter from estimated $K_d = k_1/k_2 = 6$ μM (20).
k_3	$5.25 \times 10^{-4}\ s^{-1}$	Fitted parameter from $k_3 = 0.0006$ s^{-1} (8, 21).
k_4	$5 \times 10^4\ M^{-1}s^{-1}$	Fitted parameter from $k_4 = 2.5 \cdot 10^4$ M^{-1} s^{-1} (18, 22).
k_5	$2.875 \times 10^4\ M^{-1}s^{-1}$	Fitted parameter from estimated $K_d = k_5/k_6 = 50$ μM.
k_6	$8.0 \times 10^{-2}\ s^{-1}$	Fitted parameter from estimated $K_d = k_5/k_6 = 50$ μM.
k_7	$10 \times 10^7 M^{-1}s^{-1}$	Fitted parameter from $k_7 = 7.5 \cdot 10^4$ M^{-1} s^{-1} (6).

Figure 7: Reaction parameters used in the model of Rab5 positive feedback from [1]
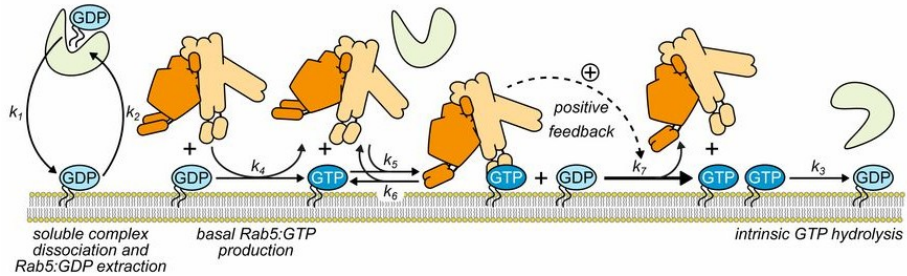

Figure 8: Schematic representation of modeled interactions from [1].

3.2 Theoretical model for Rab5/Rab11 phase separation

It has been demonstrated that active Rab11 plays a pivotal role in regulating cargo flow by recruiting the protein machinery involved in vesicle transport. Active Rab11 vesicles that have detached from peripheral endosomes accumulate on ERC membranes in a manner that depends on the action of the dynein protein. The degree of Rab11 activation serves as a determinant of the rate of membrane release destined for the ER. The evidence presented in this study lends support to the hypothesis that Rab11 activation is initiated on EE membranes, where the sorting of recycling cargoes occurs. [2]
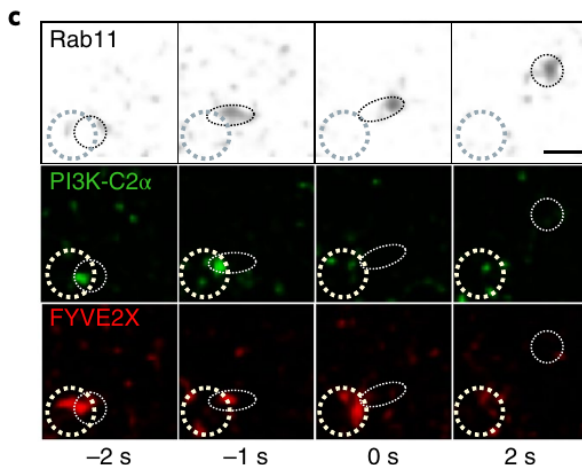
Figure 9: Fig. from [2]. Representative time-lapse series of cells co-expressing mCherry-FYVE2X, GFP-PI3K-C2α, and mECFP-Rab11 (gray scale). White circles represent membrane-bound structures.

In order to gain a deeper understanding of the relationships between the Rabs involved in the recycling route, a reaction scheme for Rab5 and Rab11 interactions has been proposed. This has been done on the basis of a previous work which analyses the formation of Rab5 and Rab7 domains [4]. Both of these proteins can exist in either an active or inactive form. Therefore, it is also necessary to consider the presence of the appropriate GAPs and GEFs. The activity of GEFs and GAPs has been modelled as a Rab GDP/GTP exchange and GTP hydrolysis: GEFs catalyse the exchange of GDP with GTP, and GAPs catalyse the hydrolysis of GTP into GDP acting upon the respective Rab proteins. Table 3 contains a list of the reactions present in the system. The molecules present on the membrane are capable of diffusing across it and transiting from the membrane to the cytosol. The two modules are connected with positive and negative feedback loops. The presence of active Rab is sufficient to activate additional Rab proteins through the action of a GEF.
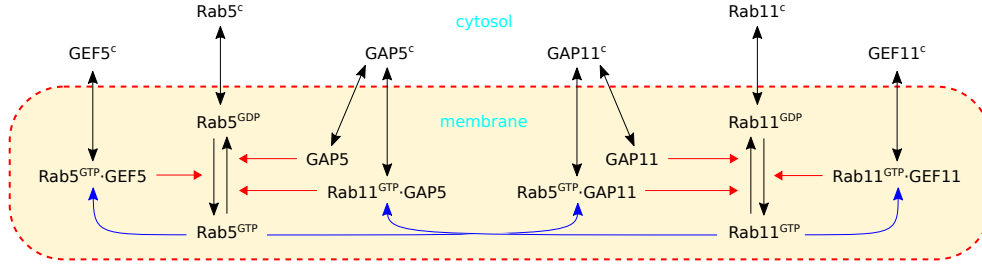
Figure 10: Representation of Rab5/Rab11 model

$Rab5^{GTP}$:GEF5 $\rightleftharpoons$ $Rab5^{GTP}$+GEF5(c)	dissociation/association	k^d_{GEF5}/k^a_{GEF5}
$Rab5^{GTP}$:GAP11 $\rightleftharpoons$ $Rab5^{GTP}$+GAP11(c)	dissociation/association	k^d_{GAP11}/k^a_{GAP11}
$Rab11^{GTP}$:GAP5 $\rightleftharpoons$ $Rab11^{GTP}$+GAP5(c)	dissociation/association	k^d_{GAP5}/k^a_{GAP5}
$Rab11^{GTP}$:GEF11 $\rightleftharpoons$ $Rab11^{GTP}$+GEF11(c)	dissociation/association	k^d_{GEF11}/k^a_{GEF11}
$Rab5^{GDP}$ $\rightleftharpoons$ $Rab5^{GDP}$(c)+b.s	dissociation/association	
$Rab11^{GDP}$ $\rightleftharpoons$ $Rab11^{GDP}$(c)+b.s	dissociation/association	
GAP5(m) $\rightleftharpoons$ GAP5(c)+b.s	dissociation/association	
GAP11(m) $\rightleftharpoons$ GAP11(c)+b.s	dissociation/association	
$Rab5^{GTP} \rightarrow Rab5^{GDP}$	catalysis $[Rab11^{GTP}$:GAP5$]$	k^c_1, K_m
$Rab5^{GTP} \rightarrow Rab5^{GDP}$	catalysis $[$GAP5(m)$]$	k^c_1, K_m
$Rab5^{GDP} \rightarrow Rab5^{GTP}$	catalysis $[Rab5^{GTP}$:GEF5$]$	
$Rab11^{GTP} \rightarrow Rab11^{GDP}$	catalysis $[Rab5^{GTP}$:GAP11$]$	k^c_3, K_m
$Rab11^{GTP} \rightarrow Rab11^{GDP}$	catalysis $[$GAP11(m)$]$	
$Rab11^{GDP} \rightarrow Rab11^{GTP}$	catalysis $[Rab11^{GTP}$:GEF11$]$	k^c_4, K_m

Table 3: List of reactions in the biochemical network (Rab5/Rab11)

4 Numerical simulations

4.1 Spatial simulations of the Rab5 model

The formation of domains on the cell's membrane can be simulated on a spherical surface lattice, through a stochastic model simulating the reactions characterising our biochemical network. The plasma membrane is represented as a sphere of radius $R = 200nm$ with a surface of the sphere ($S \approx 0.5\mu m^2$) divided in 10230 hexagons and 12 pentagons (lattice-site). The molecules in the endosome interacts with the surrounding cytosol (The volume of the cytosol can be estimated to be approximately $\approx 4000\mu m^3$). Each polygon can be occupied by an integer number of molecules, representing the concentration on that site.

The molecules on the membrane can diffuse between the sites and through the cytosol thanks to the presence of the binding site locate on the membrane, but the total number of molecules remains constant.

Parameter	Symbol	Unit of Measure
Diffusivity	D	$\mu\text{m}^2 s^{-1}$
Density (or concentration) Rab	ρ	nM
Density (or concentration) GEF	ρ	nM
Association rate	k^a	$(\text{s} \cdot \mu\text{M})^{-1}$
Dissociation rate	k^d	s^{-1}
Catalytic constant	k^c	s^{-1}
Michaelis constant	K^M	nM

Table 4: Table containing a list of parameters used in the program.

The subsequent page presents the results of the simulations pertaining to the reactions enumerated in Table 1. The simulation program accepts the reactions and corresponding rates as input. Additionally, the input quantities of the molecules at each site are provided. In this illustrative example, the initial configuration is constituted by:

Protein types	Units
$Rab5^{GTP}$	2
$Rab5^{GDP}$	2
binding-site	3
$Rab5^{GTP}$:GEF5	0
$Rab5^{GDP}$ (c)	0
Gap5(m)	0
Gap5(c)	1000
GEF5(c)	2000

Table 5: Initial condition of the various proteins employed in the simulation program for the Rab5 model.

Where the m refers to the localisation of the protein in the membrane, while c indicates that the protein is in the cytosol. When a protein is located in the membrane the corresponding unit value refers to the value per site (for example, in this initial configuration there are $2 \cdot 10242 = 20484$ units of Rab5a), while for the protein located in the cytosol the corresponding value represents the total value.

The output of the simulation program is the representation of the endosome (the sphere with 10242 sites) at different time steps. Figures 11, 12, 13 show the initial, intermediate and final stages of the simulation. It is possible to see the spatial evolution of the domain formation, starting from an initial configuration where the sphere is in a well mixed state (each site is occupied by 2 $Rab5^{GTP}$ and 2 $Rab5^{GDP}$), in the intermediate state it is possible to visualise the domain formation with some macrodomains, while in the last step (representing the steady state) only 2 larger macrodomains are visualised.
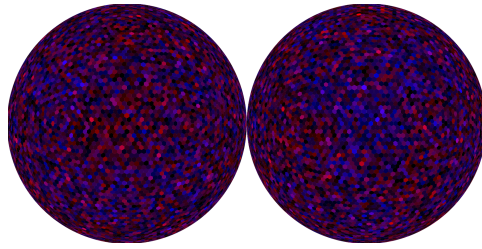
Figure 11: Rab5 model. Initial stage. Front and Back of the endosome. In blue $Rab5^{GTP}$, in red $Rab5^{GDP}$
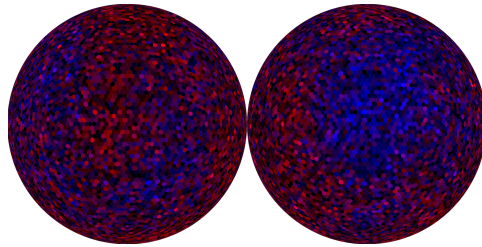

Figure 12: Rab5 model. Intermediate stage. Front and Back of the endosome. In blue $Rab5^{GTP}$, in red $Rab5^{GDP}$
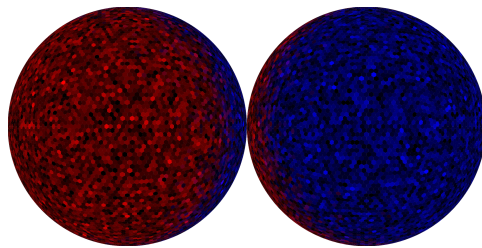

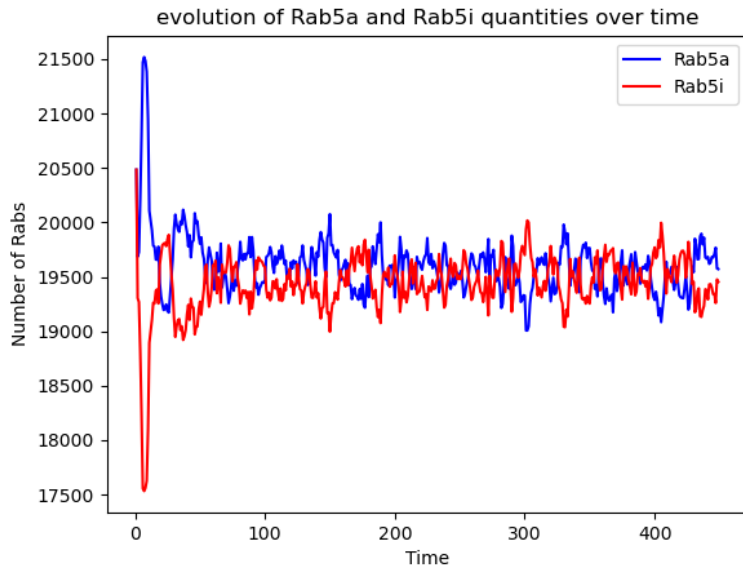Figure 13: Rab5 model. Final stage. Front and Back of the endosome. In blue $Rab5^{GTP}$, in red $Rab5^{GDP}$

Figure 14: Evolution of the quantities $Rab5^{GTP}$ and $Rab5^{GTP}$ over time

The numerical simulation of the Rab5 model reveals a dynamic progression through distinct stages of domain organization. Initially, the system exhibits a well-mixed state, characterized by a homogeneous distribution of $Rab5^{GTP}$ (depicted in blue) and $Rab5^{GDP}$ (depicted in red). As time progresses, small domains begin to form and coalesce, marking the onset of macroscopic phase separation. The growth of these domains, however, is contingent on surpassing a critical minimum size, below which they cannot stabilize and persist.

In the intermediate stage, a process of dynamic coarsening becomes evident: larger domains grow at the expense of smaller ones through a competitive mechanism, leading to a decrease in the total number of domains while simultaneously increasing their average size. This stage highlights the inherent self-organizing properties of the system as it transitions toward greater spatial organization. The self-organization observed in this stage highlights the robustness of the feedback-driven system in establishing spatial order.

Finally, in the terminal stage illustrated in Fig. 13, the system achieves a state of equilibrium, characterized by the emergence of two distinct, stable domains. These final domains represent the culmination of the phase separation process, underlining the interplay between $Rab5^{GTP}$ and $Rab5^{GTP}$ dynamics in establishing spatial organization within the membrane.

21

4.2 Spatial simulations of the Rab5/Rab11 model

As in the previous scenario, in this section the Rab5/Rab11 model was simulated to explore the underlying molecular dynamics in more detail. The reactions outlined in Table 3 were implemented using the Gillespie algorithm, enabling a stochastic simulation that captures the intricate molecular interactions and state transitions within the system.

Initial conditions:

Protein types	Units
Rab5a	2
Rab5i	0
Rab5a	2
Rab5i	0
bind-site	3
GAP5(c)	1000
GAP11(c)	1000
GEF5(c)	2000
GEF11(c)	2000

Table 6: Initial condition of the various proteins employed in the simulation program for the Rab5/Rab11 model. All the other quantities are set to zero.

The following pages present the results of the Rab5/Rab11 model simulation, offering a visual representation of the spatial organisation of $Rab5^{GTP} + Rab11^{GTP}$ and $Rab5^{GDP} + Rab11^{GDP}$ across the membrane domains. These outputs provide insights into the dynamic interplay between the active and inactive states of Rab proteins. Moreover, the time evolution of these quantities is depicted.
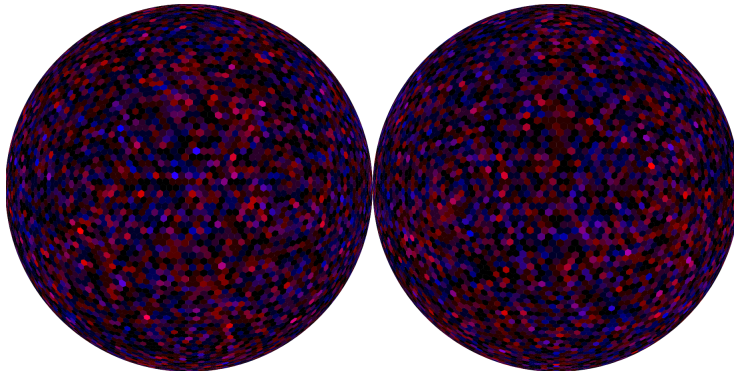
Figure 15: Rab5/Rab11 model. Initial stage. Front and Back of the endosome. In blue $Rab5^{GTP}$, in red $Rab11^{GTP}$
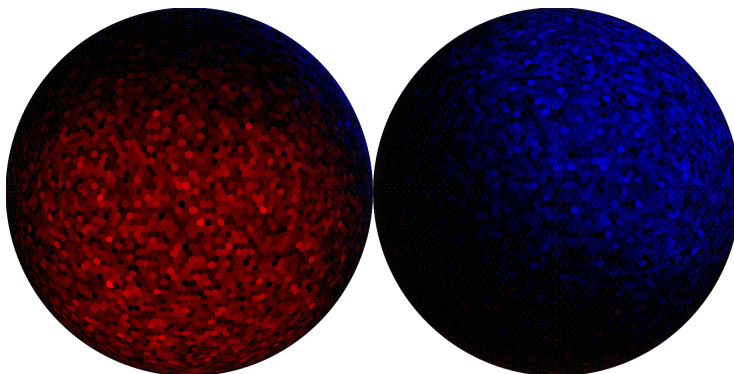

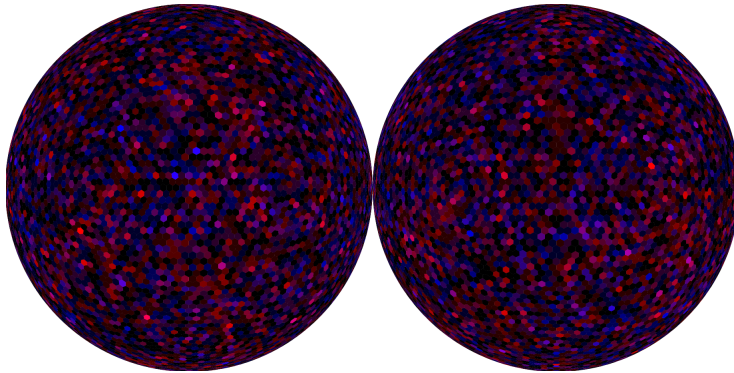Figure 16: Rab5/Rab11 model. Final stage. Front and Back of the endosome. In blue $Rab5^{GTP}$, in red $Rab11^{GTP}$

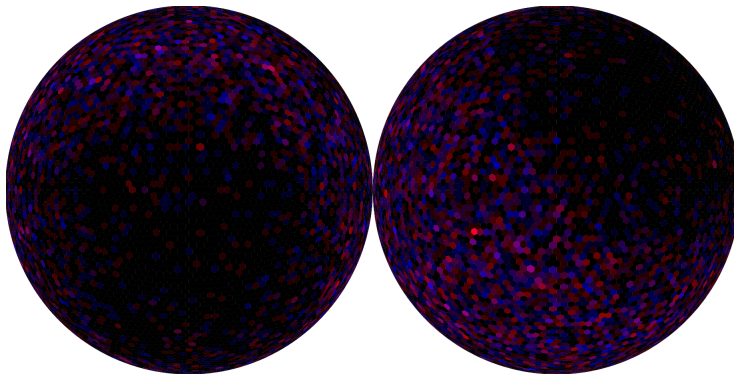Figure 17: Rab5/Rab11 model. Initial stage. Front and Back of the endosome. In blue $Rab5^{GDP}$, in red $Rab11^{GDP}$

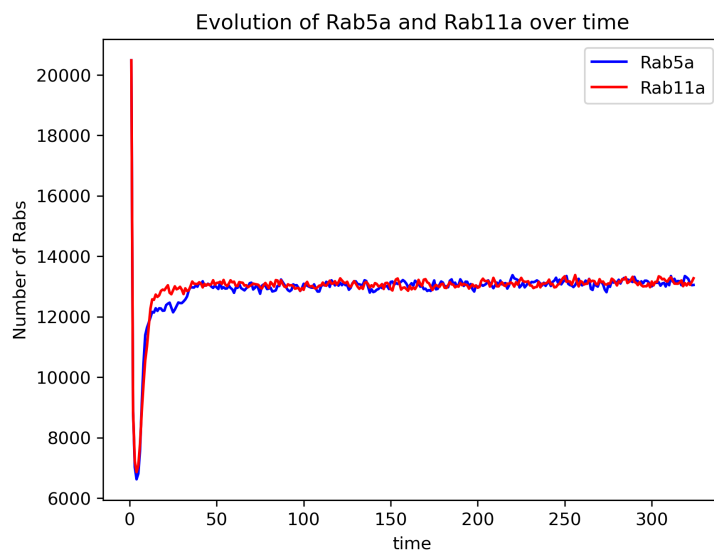Figure 18: Rab5/Rab11 model. Final stage. Front and Back of the endosome. In blue $Rab5^{GDP}$, in red $Rab11^{GDP}$

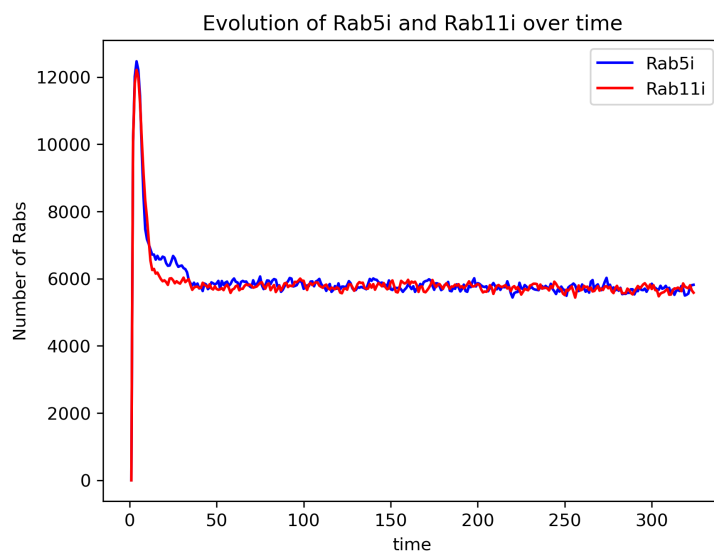Figure 19: Evolution of Rab quantities. In blue $Rab5^{GTP}$, in red $Rab11^{GTP}$.

Figure 20: Evolution of Rab quantities. In blue $Rab5^{GDP}$, in red $Rab11^{GDP}$.

From the numerical simulation of the Rab5-Rab11 model, the system evolves through distinct stages, driven by feedback interactions between the two Rab proteins. In the initial state, the system exhibits a homogeneous distribution of $Rab5^{GTP}$ (blue) and $Rab11^{GTP}$ (red) across the membrane, representing a well-mixed state. This stage is characterized by the local activation of Rab5 and Rab11 through their respective GEFs, which begins to amplify small fluctuations in their concentrations.

In the intermediate state, spatially distinct domains of $Rab5^{GTP}$ and $Rab11^{GTP}$ start to emerge, driven by feedback loops. $Rab5^{GTP}$ recruits GAP11, which inactivates Rab11 in its vicinity, while $Rab11^{GTP}$ recruits GAP5, suppressing Rab5 locally. This reciprocal inhibition creates a competitive dynamic, allowing larger domains of Rab5 and Rab11 to grow at the expense of smaller ones. This process, known as dynamic coarsening, results in a reduction in the number of domains but an increase in their size.

In the final state, the system achieves a stable configuration where two macroscopic, well-separated domains are formed: one dominated by $Rab5^{GTP}$ and the other by $Rab11^{GTP}$. These stable domains, illustrated in Fig. 16, reflect the balance between positive feedback from the GEFs and reciprocal inhibition via the GAPs, enabling a clear spatial organization of the membrane into distinct functional regions. In Fig. 18, the final stage of inactive proteins does not show the formation of distinct domains, highlighting the critical role of positive feedback loops in driving domain organization. The inactive proteins were primarily localized in areas surrounding the active domains, in a mixed Rab5/Rab11 state. However, they also showed co-localization with the active proteins. From fig. 19 and 20 it is possible to visualize the time evolution of Rab5 and Rab11 quantities. After an abrupt change in the initial quantities both the active and inactive proteins stabilize.

5 Quantitative Analysis of Rab domains on endosomal membranes

5.1 Statistical Object Distance Analysis (SODA)

If we want to understand how proteins work and how they are organised, it is essential to look at their localisation at the subcellular level. One of the most widely used methods for spatial analysis is to label proteins with different fluorophores. There are three main obstacles to the robustness of co-localisation analysis:

- image noise and background intensity

- the dependence of traditional correlation index by the PSF of the microscope

- the topological organization of molecules within the cell can bias the interpretation of correlation coefficient (molecules overloap)

The SODA method is fast becoming a key tool in the mapping of coupled objects within the cell [7]. SODA employs a marked point process framework, where the "mark" is the ensemble of features of each individual spot (such as colour, size, shape, ...), while the "Point Process" is a mathematical model that focuses the analysis within a cellular region of interest (ROI), where the localisation of spots is considered as a collection of randomly distributed points. The spots are detected by an algorithm based on a wavelength transformation of the image and statistical threshold coefficients. The centre of mass of the spots is used as the position.

The SODA method does not depend on the PSF characteristics because it focuses on analysing the spatial relationships between molecular positions, rather than the exact appearance or intensity distribution of these points in an image. The PSF affects the appearance of a molecule, but SODA analysis is based only on where the molecule is located in space (the centre of the spot is used). To detect the fluorescent spots, an automatic algorithm is used, implemented in the Icy platform as a plugin called "Spot Detector". The obtained spots correspond to the centre of mass and are used as position.

This method is based on the Ripley's K function to determine a spatial relationship between two populations:

$$K(r) = \frac{Volume\{ROI\}}{n_1 n_2} \sum_{x,y} \mathbf{1}_{d(x,y) \geq r} k(x,y)$$

$n_{i=1,2}$ Number of object n_1, n_2
$d(\mathbf{x}, \mathbf{y})$ Distance between objects
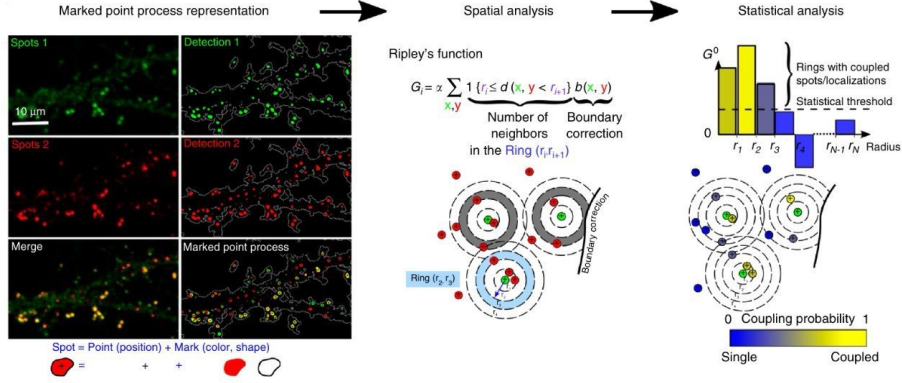$k(\mathbf{x}, \mathbf{y})$ Boundary correction

Figure 21: Fig. from [7] SODA principles: (i) Molecules are labelled with different fluorescent probes (green spots 1, red spots 2). Fluorescent spots are automatically detected and represented with a Marked Point Process. The ROI boundary is highlighted with a white dashed line. (ii) Spatial coupling between spots 1 and 2 is quantified with the Ripley's K function . (iii) Statistical threshold (black dashed line) of the (reduced) Ripley's function indicates the rings where (red) spots 2 accumulate significantly.

Given a distance r, the K(r) function is proportional to the number of A_2 objects that are located within a distance r form A_1 objects. Boundary correction in Ripley's K-function is a technique used to mitigate the distorting effects caused by the edges of the area of interest when analysing the spatial distribution of points. This problem occurs because points close to the edges of the study area have fewer neighbouring points to consider than central points, which can lead to a bias in the calculation of the K-function.

$$k(\mathbf{x}, \mathbf{y}) = \frac{volume\{C(x, d(x,y))\}}{volume\{C(x, d(x,y)) \cap ROI\}}$$

$C(x, d(x,y))$ represent the area centred on x with $d(x,y)$ as a diameter.

Another function play an important role in the spatial analysis:

$$G = [K(r_{i+1} - K(r_i)]_{i=0...N-1}$$

It counts the number of objects of one type at a given distance from objects of the other type. Under the null hypothesis, the number of red objects fluctuates around green objects. For a sufficiently number of red objects each component of G is normally distributed with $\mu_i = \pi(r_{i+i}^2 - r_i^2)$ and s.d σ_i that depends on the covariance between $K(r_i)$ and $K(r_{i+i})$.

28

To statistically detect the rings in which the coupled objects accumulate and to estimate the coupling probability of each individual pair of objects, a new vector $\mathbf{G^0}$ with zero mean and unit variance is described.

The term $\boldsymbol{G} - \boldsymbol{\mu}$ is critical for assessing whether the observed spatial distribution of objects deviates significantly from what would be expected if the objects were distributed randomly (under the null hypothesis).

$$\boldsymbol{G}^0 = \frac{1}{\boldsymbol{\sigma}} \boldsymbol{A}^{-1} [\boldsymbol{G} - \boldsymbol{\mu}]$$

$\mathbf{A}$ represent the proportion of the volume of $Ring(r_i, r_{i+1})$ that overlaps with $Ring(r_j, r_{j+1})$

$$\boldsymbol{A} = [\alpha_{i,j}]_{0 \leq i,j \leq N-1} \quad with, \ \alpha_{i,j} = \frac{Volume\{Ring(r_i, r_{i+1}) \cap Ring(r_j, r_{j+1)}\}}{Volume\{Ring(r_i, r_{i+1})\}}$$

To decide which components are significantly positive the Donho and Johnstone and hard-threshold procedure with $T(N) = \sqrt{2log(N)}$ where N represents the length of the vector G^0 . Only the values of G_i^0 with values above this threshold are the significant components.

An important parameter used to determine whether the presence of a red object inside a ring located at position x could couple with the green one located at position y is the coupling probability, which is defined as the ratio between the number of red coupled objects inside $Ring(r_i, r_{i+1})$ after correcting for ring overlap and the total number of red objects in $Ring(r_i, r_{i+1})$:

$$P(x, y) = \sum_{i=0}^{N-1} \mathbf{1}\{r_i \leq d(\boldsymbol{x}, \boldsymbol{y}) \leq r_i + 1\} \mathrm{x} \frac{\tilde{C}_i}{\text{Total n. of (red) objects in } \mathrm{Ring}(r_i, r_{i+1})}$$

$$= \sum_{i=0}^{N-1} \mathbf{1}\{r_i \leq d(\boldsymbol{x}, \boldsymbol{y}) \leq r_i + 1\} \frac{\sigma_i G_i^0 \mathbf{1}\{G_i^0 > T(N)\}}{G_i}$$

Total number of red objects inside ring $(r_i, r_{i+1}) = \frac{n_1 n_2}{\text{Volume del ROI}} G_i$

The number of (red) coupled objects inside $\mathrm{Ring}(r_i, r_{i+1})$ after correction of rings overlap is given by:

$$\tilde{C}_i = \frac{n_1 n_2 \sigma_i G_i^0}{\text{volume of the ROI}} \mathbf{1}$$

For values of the probability close to zero for each other object, it means that they are single objects. On the other hand, a probability close to 1 means that they are coupled objects.

Another index which may be of interest for analysis is:

$$Coupling\ Index(A_i) = \frac{1}{n_i} \sum_{\boldsymbol{x},\boldsymbol{y}} P(\boldsymbol{x},\boldsymbol{y})$$

Where $\sum_{\boldsymbol{x},\boldsymbol{y}} P(\boldsymbol{x},\boldsymbol{y})$ represent the total number of couples and $n_{i=1,2}$ the total number of object within population A_1 or A_2.

Thanks to the coupling probabilities between each pair of objects, it is possible to analyse other parameters such as the mean distance between the coupled objects:

$$Mean\ Coupling\ Distance = \frac{\sum_{\boldsymbol{x},\boldsymbol{y}}[P(\boldsymbol{x},\boldsymbol{y})d(\boldsymbol{x},\boldsymbol{y})]}{\sum_{\boldsymbol{x},\boldsymbol{y}} P(\boldsymbol{x},\boldsymbol{y})}$$

5.2   Analysis of experimental data

To study the Rab5 and Rab11 domains quantitatively and to observe how this domain changes when perturbed by an external agent, we analysed three different sets of images using the Icy platform [7]. The first set contains 29 images of a control system representing the basal state of the cells. The second set contains 30 images of cells treated with VPS34-IN1, a specific inhibitor that interferes with the VPS34 signalling pathway. Finally, the third set contains 30 images of cells treated with nocodazole, a microtubule destabilising agent used to study how disruption of the microtubule cytoskeleton affects the organisation of Rab5/Rab11 domains. The analysis is performed using the Icy platform, via the online protocol "Easy SODA-2 colour-1 image".

(a) Original image   (b) Spot detection
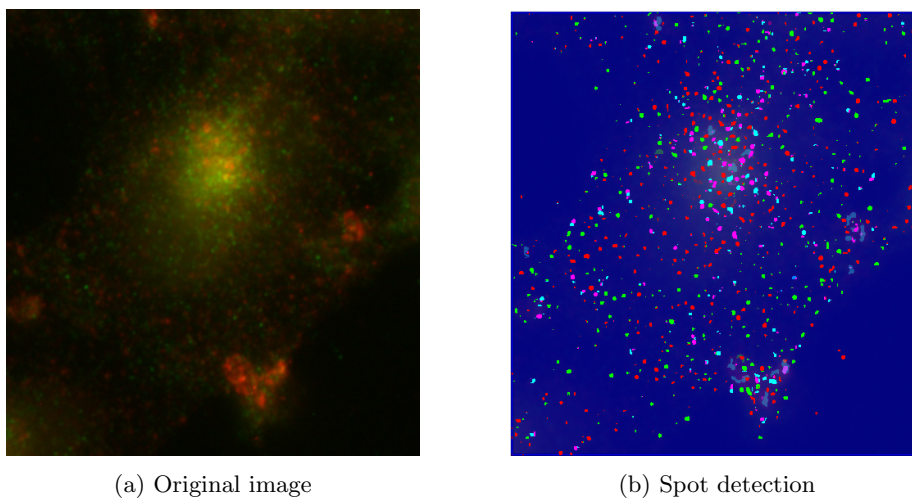
Figure 22: On the left, an example of a cell showing the distribution of Rab11 (green) and Rab5 (red). On the right, the same cell analyzed using the spot detection protocol [Isolated green spots remain green. Green spots statistically associated with red spots become cyan. Isolated red spots remain red. Red spots statistically associated with red spots become pink].

For the experiment, U251 cells were treated with either 1 µM nocodazole or 1 µM VPS34-IN1 for 3 hours. Control cells were treated with DMSO, the solvent used to dissolve the drugs, to ensure that any observed effects were attributable to the drugs and not to the solvent itself. After treatment, the cells were processed using immunofluorescence techniques. Imaging was performed using a Leica widefield microscope equipped with a 100x OIL objective lens (NA 1.30).

Each image of the different sets has been analysed and different types of data have been collected. In our case, we used the following data:

1. Total number of detections 1 inside the selected ROIs of the image

2. Total number of detections 2 inside the selected ROIs of the image

3. Total number of spots 1 that are coupled with at least one spot 2

4. Total number of spots 2 that are coupled with at least one spot 1.

5. Distances expressed in pixel between coupled spots.

To perform the spot detection of the image, the protocol uses the Spot Detector plugin. The whole area of the image is selected as ROI (region of interest). The output of the analysis also reports the coordinate (x,y) and the number of pixels of each spot.

The analysis was performed for different radii around the centre of the spot: $\mathbf{r} = [\ 1;\ 2;\ 3;\ 4;\ 5]$ (pixel). However, only $r = 3$, $r = 4$ and $r = 5$ were considered, as the image resolution is 200 nm with a pixel size of approximately 100 nm. The maximum radius, $r = 5$, was chosen to encompass endosomes up to 500 nm in size.

To check whether there are differences between the composition of the Rab5 and Rab11 domains in the cell in the untreated and treated case (with Nocodazolo and Vps34-IN1), the total number of Rab5 and Rab11 is first compared. Then the total number of green spots (Rab11) coupled with at least one red spot (Rab5) was normalised with respect to the total number of Rab11. In the same way, the total number of red spots (Rab5) that are coupled with at least one green spot (Rab11) has been normalised with respect to the total number of Rab5. In this way it is possible to compare the normalised mean of the coupled Rab. This procedure has been done for the different radii , $r = 3$, $r = 4$ and $r = 5$. The same procedure is used to analyse the distances (expressed in pixels) between Rab11 and Rab5 pairs.The same procedure is used to analyse the distances (expressed in pixels) between Rab11 and Rab5 pairs.

5.2.1 Treatment with the PI3-kinase class III inhibitor Vps34-IN1

The VPS34, a catalytic component of class III hosphatidylinositol-3- phosphate kinase (PI3Ks) complex, has been the subject of several studies because it is involved in the production of Phosphatidylinositol-3-phosphate (PI3P) [10]. PI3P is one of the most important tag for early endosomes. Endocytosed membranes are initially gathered in peripheral membranous structures, referred to as pre-early endosomes (pre-EEs), and then mature into early endosomes (EEs) through the acquisition of Rab5 and the subsequent recruitment of Vps34. The Vps34 phosphorylates PI at the 3' position to generate PI3P at membranes. PI3P is required for the recruitment of proteins needed for the maturation of EEs (including homotypic fusion, cargo sorting, plus-end-directed movements along the microtubule, tubulation, and the development of outgoing endosomal carriers in various directions). PI3P serves as a pivotal regulator of Rab5 activity by driving its recruitment to membranes via a positive feedback loop that engages the GEF/effector complex Rabex5/Rabaptin5. This feedback mechanism is further reinforced by the interaction between Rab5 and Vps15, a subunit of the Class III PI3K complex, which stabilizes the Vps34 and enhances PI3P production at endosomal membranes. The locally generated PI3P not only stabilizes Rab5 on the membrane but also amplifies the recruitment of Rabex5/Rabaptin5, thereby sustaining Rab5 activation and the establishment of Rab5-enriched membrane domains. This dynamic interplay between Rab5, PI3P, and the Vps15-Vps34 complex ensures the functional integrity and specificity of endosomal trafficking processes [16].

The maturation of EEs involves a reconfiguration of domains of the membrane. For example Rab5 is replaced by Rab4 or Rab11 to generate tubular recycling endosomes. The conversion is associated with the decrease of Vps34.

The Vps34-IN1 reduced the number of Vps34-dependent PI3P. A prominent characteristic of enlarged Rab5 endosomes in PI3P-depleted cells is delayed maturation along both EE-to-LE pathways. The maturation process of Rab5 domains depends on PI3P, produced by Vps34, to deactivate Rab5 activity; a Vps34 knockdown disrupts this regulation. Knockout studies suggest that Vps34-derived PI(3)P directly regulates Rab5 activity via PI(3)P-dependent recruitment of Rab5-GAP, creating a negative feedback loop [8]. The data presented in this paper [10], which focuses on the effect of Vps34-IN1 on Rab GTPase proteins, showed that the colocalisation between Rab5a and Rab11 decreases. While the presence of Rab11 in Rab5-rich early endosomes (EEs) has been demonstrated, where it is recognized that Rab11 can recruit Rab11 GAP to prevent its activation, knowledge regarding the mechanisms of Rab11 activation is limited. It has been demonstrated that Rab11 co-localize with Rab5 in the cell periphery, on the same way Rab11 co-localize with PI3P in the cell periphery, indicating that peripherally located early endosomes (PE) in which active Rab11 colocalized with PtdIns(3)P correspond to early endosomes. Rab11 positive endosome appared to be enlarged, vacuolized and displaced from the cell center around the nucleous in a ring-like pattern [10].
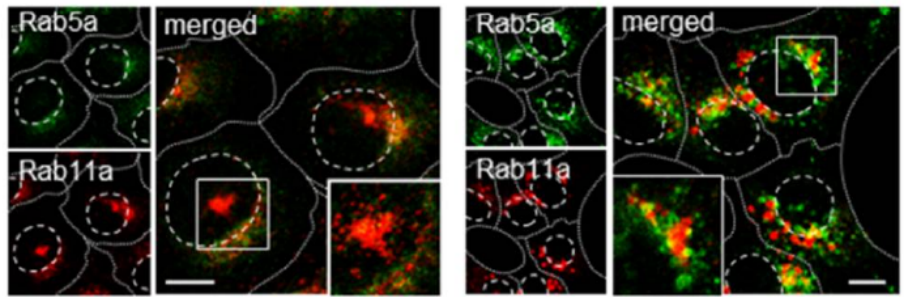
Figure 23: Co-localization images of Rab5 adn Rab11. On the left the control is visualized. On the right the cells are treated for 60 min with 3 μM. Cell borders are indicated by fine dotted lines and cell nuclei by fine dashed lines [10]

In the set of images of cells treated with Vps34-IN1, we investigated the effect of the treatment on the total levels of Rab5 and Rab11 compared to the control condition. As shown in the barplot in Figure 24, there is a decrease in the mean level of Rab11 in the treated cells compared to the control, suggesting a possible effect of Vps34-IN1 on Rab11 expression. In contrast, Rab5 levels remain relatively stable, indicating that the treatment does not significantly alter Rab5 abundance under the conditions tested.
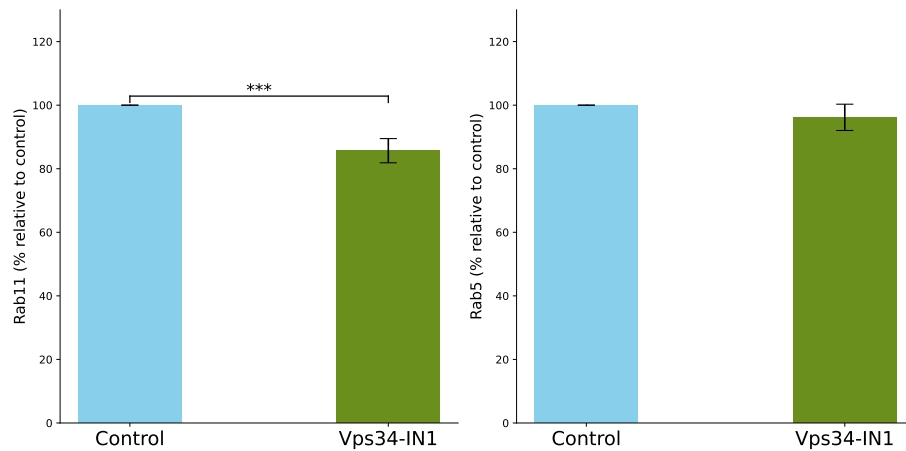
Figure 24: Comparison of Rab11 and Rab5 levels in cells treated with Vps34-IN1 relative to the control. Values are expressed as a percentage relative to the control (the red dashed line represents 100 %). Left: Level of Rab11 in Nocodazole-treated cells (One sample t-test: t = -3.762, p = 0.0008268; *** $p < 0.001$). Right: Level of Rab5 in Nocodazole-treated cells (One sample t-test: t = -0.926, p = 0.3628).

The distribution of Rab11, normalised to the total number of Rab11 in each cell, in the vicinity of Rab5 was then analysed. The boxplots in Figures 36, 37 and 25 illustrate this distribution for both Vps34-IN1-treated cells and control cells at different radii: $r = 3$, $r = 4$, $r = 5$. These comparisons allow us to observe how the spatial relationship between Rab11 and Rab5 changes under Vps34-IN1 treatment at different distances. It can be observed that the composition of Rab5 and Rab 11 domains remains approximately the same, except in the case of fig. 25 (r=5), where there is a decrease of Rab5/Rab11 co-localization.
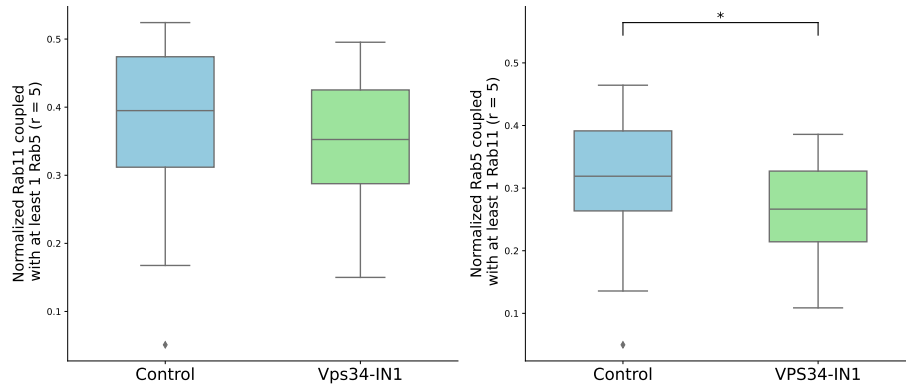
Figure 25: Left: Boxplot comparing the distribution of normalized Rab11 coupled with at least 1 Rab5 (r = 5) in control and Vps34-IN1 treated cells (Kolmogorov-Smirnov test (KS) KS = 0.247, p = 2.835e-01). The median value is indicated by the horizontal line within each box, while the box edges represent the interquartile range (IQR) from the 25th to the 75th percentile. Whiskers extend up to 1.5 times the IQR. Right: Boxplot comparing the distribution of normalized Rab5 coupled with at least 1 Rab11 (r = 5) in control and Nocodazole-treated cells (Kolmogorov-Smirnov KS = 0.348, p = 4.602e-01; * $p < 0.05$).
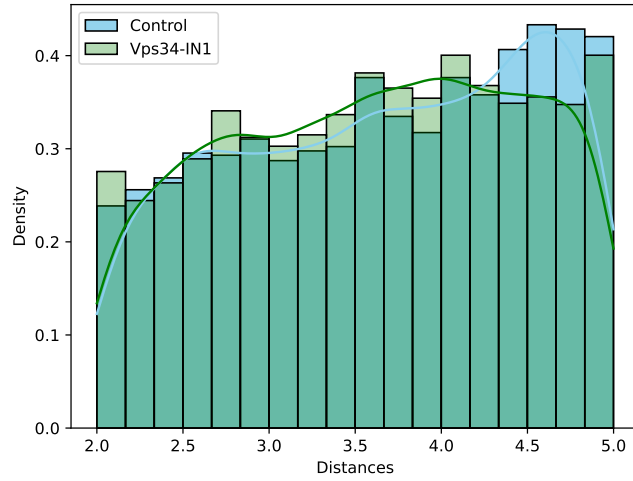
Figure 26: Comparison of distances (expressed in pixels) between pairs of Rab11 and Rab5 in Control and treated case.

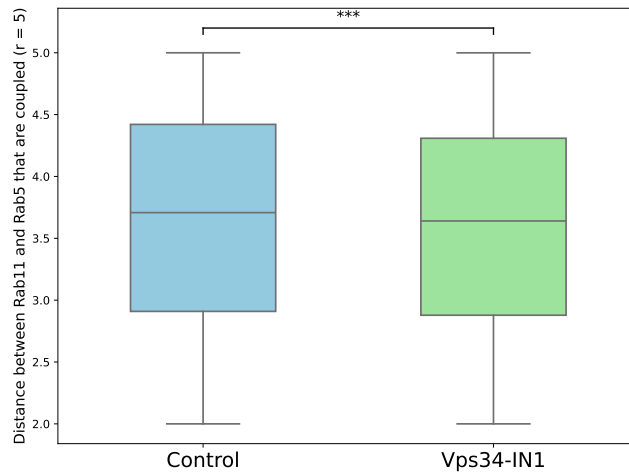
Figure 27: Boxplot comparing the density of distances between Rab11 and Rab5 couples in control and Vps34-IN1 treated cells (r=5). The median value is indicated by the horizontal line within each box, while the box edges represent the interquartile range (IQR) from the 25th to the 75th percentile. Whiskers extend up to 1.5 times the IQR (Kolmogorov-Smirnov test (KS) KS = 0.043, p = 2.416e-04; *** p < 0.001).

The histograms illustrate the distribution of distances between pairs of Rab11 and Rab5 under both control and treated conditions. This visualisation enables a comprehensive comparative analysis of the spatial organisation of these proteins, providing insights into how the treatment affects their relative positioning. By juxtaposing the two conditions, the graph highlights potential alterations in protein distribution that may reflect underlying changes in cellular processes.

To assess the spatial organization of Rab5 and Rab11 clusters, a Kolmogorov-Smirnov (KS) test was performed to compare the distributions of distances between these clusters under different experimental conditions. The KS test was chosen because it is a non-parametric test that does not assume a specific distribution for the data, making it particularly useful for comparing distributions of distances without relying on assumptions of normality. By applying the KS test, we can determine whether the distribution of distances between Rab5 and Rab11 clusters differs significantly between the control and drug-treated groups.

The results from the KS test allow us to assess whether the pharmacological treatment, such as Vps34-IN1, induces a statistically significant change in the distribution of distances between the clusters. A significant difference in the distribution would suggest that the treatment has altered the spatial organization of Rab domains, potentially reflecting changes in phase separation. For instance, a reduction in the distance between Rab5 and Rab11 clusters could indicate a disruption in their functional segregation, providing evidence of changes in the phase separation dynamics on the endosomal membrane. In Fig. 27, the Kolmogorov-Smirnov (KS) test indicates a p-value lower than 0.001, highlighting a statistically significant difference in the distribution of distances between the analyzed data. This result suggests that the treatment induces measurable alterations in the spatial organization of Rab5 and Rab11 clusters. However, it is important to note that statistical significance, as detected by the KS test, may reflect subtle differences in the overall shape of the distributions, which are not always evident in summary visualizations such as boxplots, but appear in fig. 26 .

5.2.2   Treatment with microtubule inhibitor Nocodazole

Rab11 vesicles, associated with a GTPase protein involved in endocytic re-
cycling, detach from peripheral endosomes and move toward the Endocytic
Recycling Compartment (ERC) membranes. This movement is facilitated by
dynein, a motor protein that transports vesicles along microtubules toward the
centrosome, i.e., toward the center of the cell. Dynein enables these vesicles to
accumulate at the ERC, where recycled molecules are processed before being
sent back to the plasma membrane. This recycling process helps maintain a
balanced composition of necessary molecules on the cell surface.

When Nocodazole, a compound that destabilizes microtubules, is introduced,
it can disrupt the transport of Rab11 vesicles to the ERC by inhibiting the mi-
crotubules essential for dynein-mediated movement. Under normal conditions,
dynein uses microtubules as "tracks" to move Rab11 vesicles toward the recy-
cling compartment (ERC) in the cell center. However, when Nocodazole desta-
bilizes the microtubules, this transport is compromised, significantly interfering
with intracellular recycling traffic. The treatment with nocodazole, which de-
polymerizes microtubules, leads to the accumulation of enlarged or clustered
Rab5-positive endosomes at the extreme periphery of the cell. Microtubule net-
works contribute to the intracellular distribution of Rab5-positive endosomes
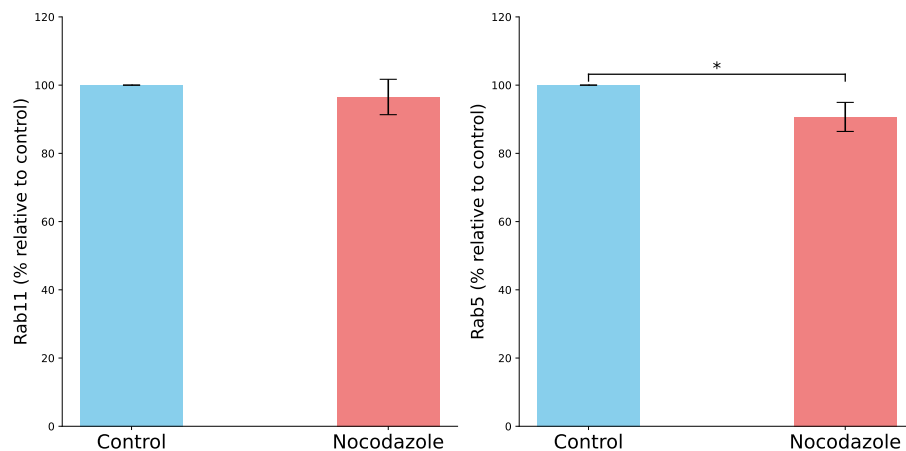[11].

Figure 28: Comparison of Rab11 and Rab5 levels in cells treated with Noco-
dazole relative to the control. Values are expressed as a percentage relative to
the control (the red dashed line represents 100 %). Left: Level of Rab11 in
Nocodazole-treated cells (One sample t-test: t = -0.670, p = 0.5084). Right:
Level of Rab5 in Nocodazole-treated cells (One sample t-test: t = -2.188, p =
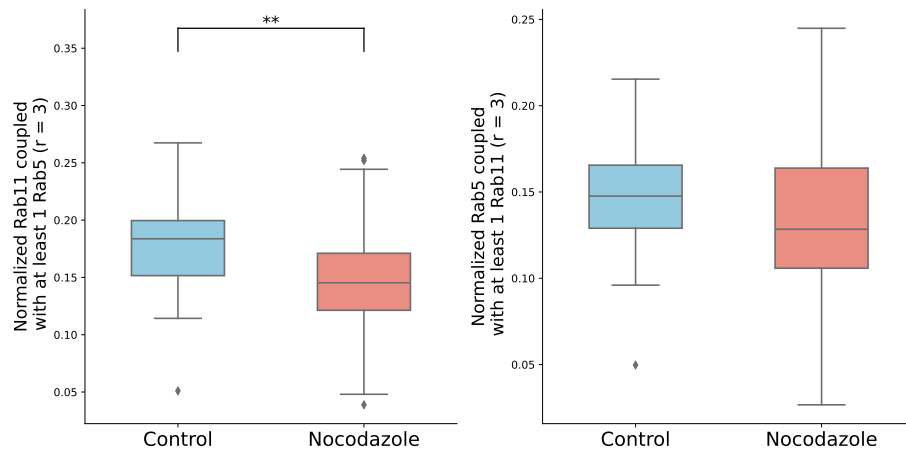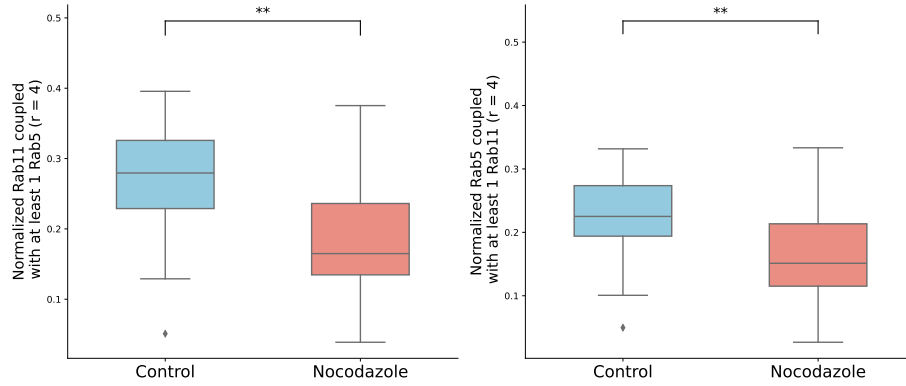0.03748; * $p < 0.05$).

Figure 29: Left: Boxplot comparing the distribution of normalized Rab11 coupled with at least 1 Rab5 (r = 3) in control and Vps34-IN1 treated cells (Kolmogorov-Smirnov test (KS) KS = 0.424, p = 6.548e-03; ** $p < 0.01$) . The median value is indicated by the horizontal line within each box, while the box edges represent the interquartile range (IQR) from the 25th to the 75th percentile. Whiskers ex- tend up to 1.5 times the IQR. Right: Boxplot comparing the distribution of normalized Rab5 coupled with at least 1 Rab11 (r = 3) in control and Nocodazole- treated cells (Kolmogorov-Smirnov KS = 0.294, p = 1.103e-01).
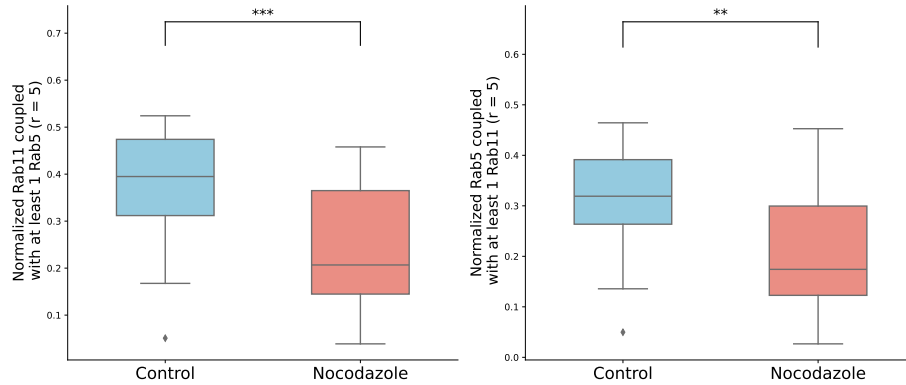
Figure 30: Left: Boxplot comparing the distribution of normalized Rab11 coupled with at least 1 Rab5 (r = 4) in control and Vps34-IN1 treated cells (Kolmogorov-Smirnov test (KS) KS = 0.491, p = 1.004e-03; ** $p < 0.01$). . The median value is indicated by the horizontal line within each box, while the box edges represent the interquartile range (IQR) from the 25th to the 75th percentile. Whiskers ex- tend up to 1.5 times the IQR. Right: Boxplot comparing the distribution of normalized Rab5 coupled with at least 1 Rab11 (r = 4) in control and Nocodazole- treated cells (Kolmogorov-Smirnov KS = 0.459, p = 2.404e-03; ** $p < 0.01$).

Figure 31: Left: Boxplot comparing the distribution of normalized Rab11 coupled with at least 1 Rab5 (r = 5) in control and Nocodazole-treated cells (Kolmogorov-Smirnov test (KS) KS = 0.494, p = 6.978e-04; *** $p < 0.001$). The median value is indicated by the horizontal line within each box, while the box edges represent the interquartile range (IQR) from the 25th to the 75th percentile. Whiskers extend up to 1.5 times the IQR. Right: Boxplot comparing the distribution of normalized Rab5 coupled with at least 1 Rab11 (r = 5) in control and Nocodazole-treated cells (Kolmogorov-Smirnov KS = 0.428, p = 4.988e-03; ** $p < 0.01$).
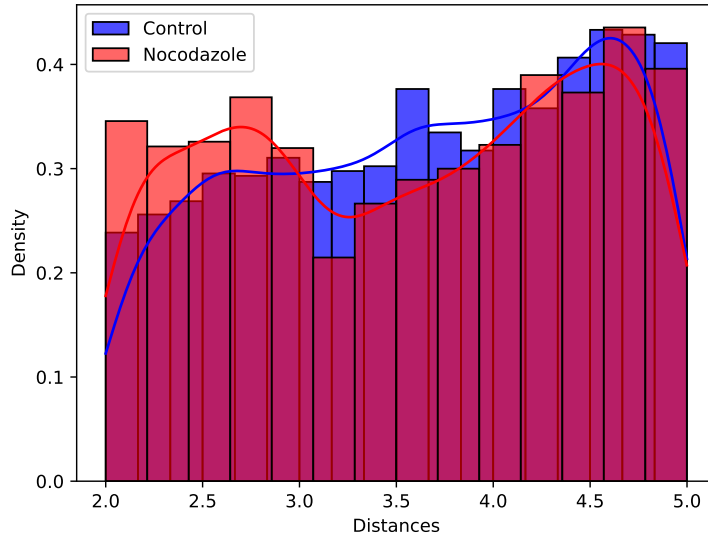
41

Figure 32: Comparison of distances (expressed in pixels) between pairs of Rab11 and Rab5 in Control and treated case

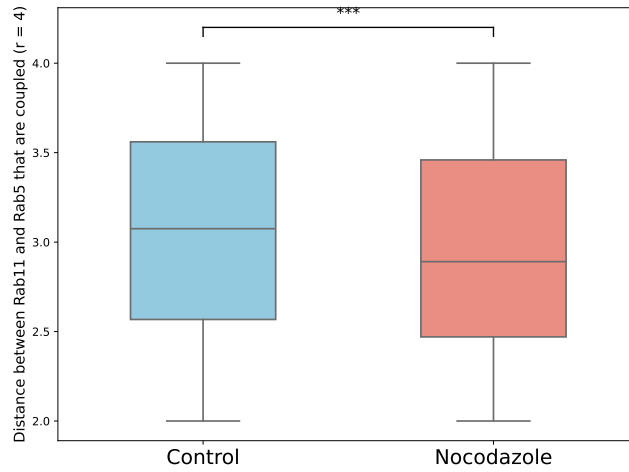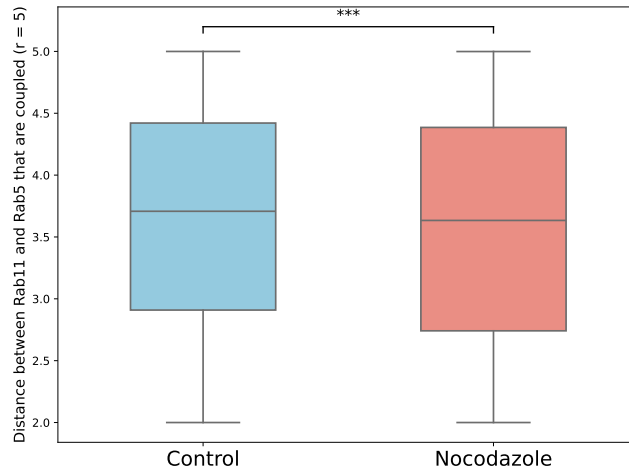
Figure 33: Boxplot comparing the density of distances between Rab11 and Rab5 couples in control and Nocodazole-treated cells (r=4). The median value is indicated by the horizontal line within each box, while the box edges represent the interquartile range (IQR) from the 25th to the 75th percentile. Whiskers extend up to 1.5 times the IQR.(Kolmogorov-Smirnov test (KS) KS = 0.100, p = 1.419e-10; *** p < 0.001)

Figure 34: Boxplot comparing the density of distances between Rab11 and Rab5 couples in control and Nocodazole-treated cells (r=5). The median value is indicated by the horizontal line within each box, while the box edges represent the interquartile range (IQR) from the 25th to the 75th percentile. Whiskers extend up to 1.5 times the IQR.(Kolmogorov-Smirnov test (KS) KS = 0.064, p = 2.248e-07; *** p <0.001)

In the Nocodazole treatment, the changes in the spatial organization of Rab5/Rab11 domains are more pronounced. This is evidenced by the statistical significance observed in the Kolmogorov-Smirnov (KS) test for distances starting from 300 nm, indicating a measurable alteration in their spatial distribution.

6 Conclusions

The mechanism of phase separation emerges as a pivotal process in the spatial and functional organization of Rab domains. By promoting the segregation of Rab proteins and their effectors into distinct membrane microdomains, phase separation ensures specificity in vesicular trafficking while minimizing functional overlap between Rab-regulated pathways. This dynamic compartmentalization enhances vesicle docking, fusion, and transport efficiency, underscoring the adaptability of cellular trafficking systems in response to changing physiological conditions. Furthermore, unraveling the interplay between phase separation and Rab protein functionality offers valuable insights into the molecular basis of endosomal organization, with broader implications for cellular homeostasis and disease pathogenesis.

If two Rab proteins are observed in close proximity within the same membranous space, under conditions where endosomes are sufficiently spaced beyond their characteristic size, it can be hypothesized that this proximity is not random. Instead, it may reflect a specific spatial organization indicative of phase separation within the endosomal membrane. In this context, phase separation does not imply a rigid physical compartmentalization but rather a functional segregation driven by molecular interactions between Rab proteins, their effectors, and membrane lipids. This segregation likely arises from self-organizing dynamics, mediated by weak and cooperative interactions, which result in the formation of distinct microdomains on the endosomal surface.

The aim of these experiments is to develop a quantitative method to measure the degree of phase separation, using Rab domains as a model system, by analyzing cells that are perturbed with specific pharmacological treatments. Treatments such as the Vps34 inhibitor (Vps34-IN1), which modulates phosphoinositide synthesis and consequently impacts lipid-protein interactions, provide a valuable opportunity to study how phase separation is regulated at the molecular level. Preliminary results indicate that, in the presence of Vps34-IN1, a decrease in the distance between Rab5 and Rab11 clusters is observed. This suggests a link between the degree of phase separation and pharmacological treatment, potentially reflecting alterations in the spatial organization and functional dynamics of endosomal domains.

One of the current limitations of this study is the spatial resolution of the imaging techniques employed, which is constrained by the diffraction limit (250 nm). This restriction complicates the precise identification of phase separation phenomena, especially when endosomes have dimensions close to this resolution limit. The application of super-resolution imaging techniques could provide more detailed and sensitive data to further investigate these processes. Additionally, exploring the modulatory effects of pharmacological treatments, such as varying the dose of Vps34-IN1, would allow a more comprehensive understanding of the correlation between the drug and phase separation.

In addition, the availability of a programme capable of simulating domain formation provides a powerful tool for improving the interpretation of exper-

imental results. By incorporating more detailed quantitative data, this programme could be used in a more refined and targeted way to generate predictive models. These simulations would not only deepen our understanding of the mechanisms driving domain organisation, but would also generate testable hypotheses, providing a framework to guide future experimental investigations. Although preliminary, these results highlight the potential of this approach to quantify the degree of phase separation in Rab domains. Encouragingly, this opens the door to further studies aimed at developing a robust quantitative phenotype to characterise phase separation and its regulation by chemical or genetic modulation.

A   Appendix

The simulation program also generates the detailed configuration of the organisation of each site. It reproduces a txt file indicating the total number of molecules present at a given time step and a second txt file indicating the number of molecules present at each site for every time step.

(a) Detailed configuration

(b) Global configuration

Figure 35: Example of a txt output file describing the configuration at time 00:08:20.

B Appendix

This appendix contains additional data analysis. Comparison for r=3 and r=4 does not shows significant differences between control and treated case (figs. 36 -40).
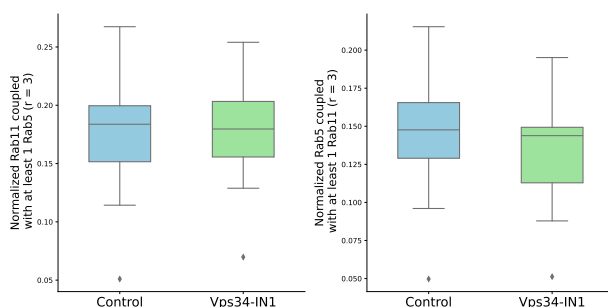

Figure 36: Left: Boxplot comparing the distribution of normalized Rab11 coupled with at least 1 Rab5 (r = 3) in control and Vps34-IN1 treated cells (Kolmogorov-Smirnov test (KS) KS = 0.106, p = 9.865e-01). The median value is indicated by the horizontal line within each box, while the box edges represent the interquartile range (IQR) from the 25th to the 75th percentile. Whiskers extend up to 1.5 times the IQR. Right: Boxplot comparing the distribution of normalized Rab5 coupled with at least 1 Rab11 (r = 3) in control and Nocodazole-treated cells (Kolmogorov-Smirnov KS = 0.279, p = 1.708e-01).
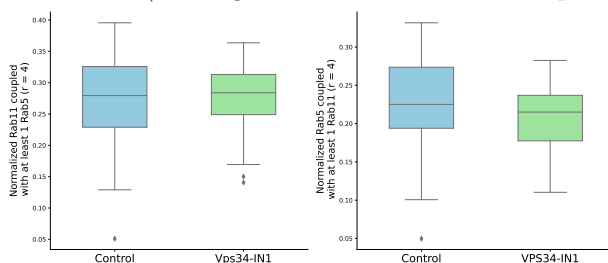

Figure 37: Left: Boxplot comparing the distribution of normalized Rab11 coupled with at least 1 Rab5 (r = 4) in control and Vps34-IN1 treated cells (Kolmogorov-Smirnov test (KS) KS = 0.146, p = 8.546e-01). The median value is indicated by the horizontal line within each box, while the box edges represent the interquartile range (IQR) from the 25th to the 75th percentile. Whiskers extend up to 1.5 times the IQR. Right: Boxplot comparing the distribution of normalized Rab5 coupled with at least 1 Rab11 (r = 4) in control and Nocodazole-treated cells (Kolmogorov-Smirnov KS = 0.248, p = 2.773e-01).
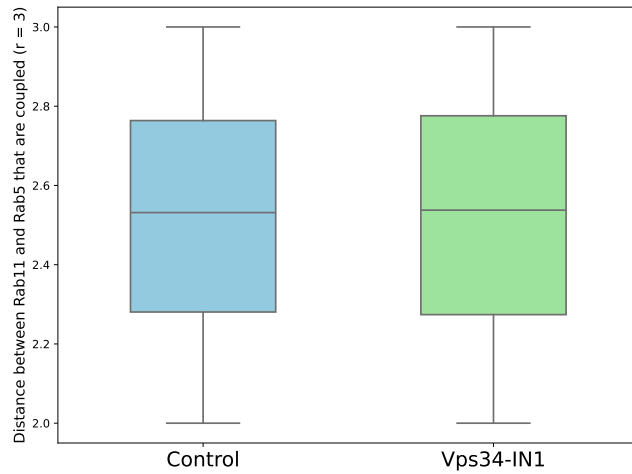
Figure 38: Boxplot comparing the density of distances between Rab11 and Rab5 couples in control and Vps34-IN1 treated cells (r=3). The median value is indicated by the horizontal line within each box, while the box edges represent the interquartile range (IQR) from the 25th to the 75th percentile. Whiskers extend up to 1.5 times the IQR.(Kolmogorov-Smirnov test (KS) KS = 0.034, p = 4.078e-01
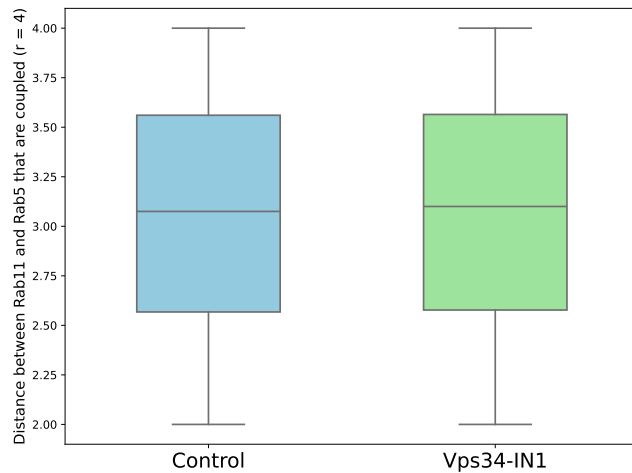

Figure 39: Boxplot comparing the density of distances between Rab11 and Rab5 couples in control and Vps34-IN1 treated cells (r=4). The median value is indicated by the horizontal line within each box, while the box edges represent the interquartile range (IQR) from the 25th to the 75th percentile. Whiskers extend up to 1.5 times the IQR.(Kolmogorov-Smirnov test (KS) KS = 0.021, p = 5.138e-01
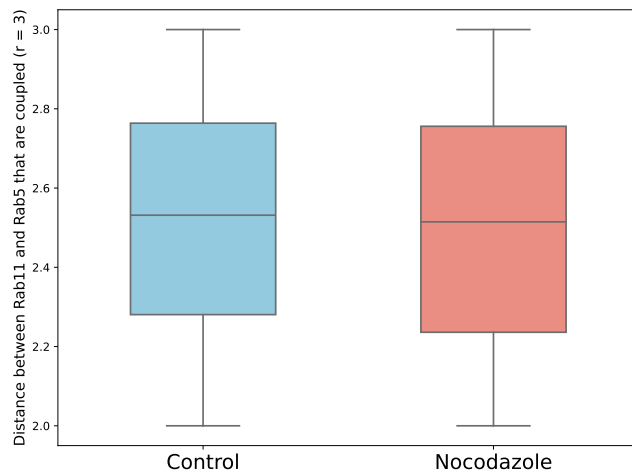
Figure 40: Boxplot comparing the density of distances between Rab11 and Rab5 couples in control and Nocodazole treated cells (r=3). The median value is indicated by the horizontal line within each box, while the box edges represent the interquartile range (IQR) from the 25th to the 75th percentile. Whiskers extend up to 1.5 times the IQR.(Kolmogorov-Smirnov test (KS) KS = 0.051, p = 7.807e-02

References

[1] Urban Bezeljak, Hrushikesh Loya, Beata Kaczmarek, Timothy E Saunders, and Martin Loose. Stochastic activation and bistability in a Rab GTPase regulatory network. *Proceedings of the National Academy of Sciences*, 117(12):6540–6549, 2020.

[2] Carlo Cosimo Campa, Jean Piero Margaria, Abhishek Derle, Marco Del Giudice, Maria Chiara De Santis, Luca Gozzelino, Francesca Copperi, Carla Bosia, and Emilio Hirsch. Rab11 activity and PtdIns (3) P turnover removes recycling cargo from endosomes. *Nature chemical biology*, 14(8):801–810, 2018.

[3] Alice Cezanne, Janelle Lauer, Anastasia Solomatina, Ivo F Sbalzarini, and Marino Zerial. A non-linear system patterns Rab5 GTPase on the membrane. *Elife*, 9:e54434, 2020.

[4] Perla Del Conte-Zerial, Lutz Brusch, Jochen C Rink, Claudio Collinet, Yannis Kalaidzidis, Marino Zerial, and Andreas Deutsch. Membrane identity and GTPase cascades regulated by toggle and cut-out switches. *Molecular systems biology*, 4(1):206, 2008.

[5] Elisa Floris, Andrea Piras, Luca Dall'Asta, Andrea Gamba, Emilio Hirsch, and Carlo C Campa. Physics of compartmentalization: How phase separation and signaling shape membrane and organelle identity. *Computational and Structural Biotechnology Journal*, 19:3225–3233, 2021.

[6] Andrea Gamba, Antonio De Candia, Stefano Di Talia, Antonio Coniglio, Federico Bussolino, and Guido Serini. Diffusion-limited phase separation in eukaryotic chemotaxis. *Proceedings of the National Academy of Sciences*, 102(47):16927–16932, 2005.

[7] Thibault Lagache, Alexandre Grassart, Stéphane Dallongeville, Orestis Faklaris, Nathalie Sauvonnet, Alexandre Dufour, Lydia Danglot, and Jean-Christophe Olivo-Marin. Mapping molecular assemblies with fluorescence microscopy and object-based spatial statistics. *Nature communications*, 9(1):698, 2018.

[8] Fiona Law, Jung Hwa Seo, Ziqing Wang, Jennifer L. DeLeon, Yousstina Bolis, Ashley Brown, Wei-Xing Zong, Guangwei Du, and Christian E. Rocheleau. The VPS34 PI3K negatively regulates RAB-5 during endosome maturation. *Journal of Cell Science*, 130(12):2007–2017, 4 2017.

[9] Rong Li and Bruce Bowerman. Symmetry breaking in biology. *Cold Spring Harbor perspectives in biology*, 2(3):a003475, 2010.

[10] Marina Marcelić, Hana Mahmutefendić Lučin, Antonija Jurak Begonja, Gordana Blagojević Zagorac, and Pero Lučin. Early endosomal VPS34-Derived Phosphatidylinositol-3-Phosphate is indispensable for the biogenesis of the endosomal recycling compartment. *Cells*, 11(6):962, 3 2022.

[11] Erik Nielsen, Fedor Severin, Jonathan M. Backer, Anthony A. Hyman, and Marino Zerial. Rab5 regulates motility of early endosomes on microtubules. *Nature Cell Biology*, 1(6):376–382, 9 1999.

[12] Mary J O'sullivan and Andrew J Lindsay. The endosomal recycling pathway—at the crossroads of the cell. *International journal of molecular sciences*, 21(17):6074, 2020.

[13] Matteo Semplice, Andrea Veglio, Giovanni Naldi, Guido Serini, and Andrea Gamba. A bistable model of cell polarity. *PLoS ONE*, 7(2):e30977, 2 2012.

[14] Harald Stenmark. Rab GTPases as coordinators of vesicle traffic. *Nature reviews Molecular cell biology*, 10(8):513–525, 2009.

[15] Birte Sönnichsen, Stefano De Renzis, Erik Nielsen, Jens Rietdorf, and Marino Zerial. Distinct membrane domains on endosomes in the recycling pathway visualized by multicolor imaging of Rab4, Rab5, and Rab11. *The Journal of cell biology*, 149(4):901–914, 2000.

[16] Shirley Tremel, Yohei Ohashi, Dustin R. Morado, Jessie Bertram, Olga Perisic, Laura T. L. Brandt, Marie-Kristin Von Wrisberg, Zhuo A. Chen, Sarah L. Maslen, Oleksiy Kovtun, Mark Skehel, Juri Rappsilber, Kathrin Lang, Sean Munro, John A. G. Briggs, and Roger L. Williams. Structural basis for VPS34 kinase activation by Rab1 and Rab5 on membranes. *Nature Communications*, 12(1), 3 2021.

[17] Ingrid R. Vetter and Alfred Wittinghofer. The Guanine Nucleotide-Binding Switch in three dimensions. *Science*, 294(5545):1299–1304, 11 2001.